ENT000556
Submitted: August 20, 2012

Proceedings of the 12th International Conference on
Environmental Degradation of Materials in Nuclear Power System – Water Reactors –
Edited by T.R. Allen, P.J. King, and L. Nelson ***TMS (The Minerals, Metals & Materials Society), 2005***

EFFECT OF THE CHROMIUM CONTENT AND STRAIN ON THE CORROSION OF NICKEL BASED ALLOYS IN PRIMARY WATER OF PRESSURIZED WATER REACTORS

F. Delabrouille[1,3], L. Legras[1], F. Vaillant[1], P. Scott[2], B.Viguier[3], E. Andrieu[3]

[1] EDF (Electricité De France) R&D, MMC, Site des Renardières, Moret sur Loing cedex 77818, France
[2] Framatome-ANP, Tour Areva, 92084 Paris La Défense cedex, France
[3] CIRIMAT – UMR CNRS 5085, ENSIACET, 118 route de Narbonne, 31077 Toulouse cedex 4, France

Keywords: nickel alloys, SCC, corrosion, chromium.

Abstract

Chromium is known to enhance the corrosion and stress corrosion cracking behaviour of nickel-based alloys in high temperature water. A study has been launched to characterize these effects for alloys containing chromium concentrations ranging from 5% to 30%. This present paper compares the growth of oxide scale in these alloys in PWR primary water, and investigates the effects of applied stress. A detailed characterization of the oxide scale is performed by SEM, TEM and SIMS. Increasing chromium content results in an increase in chromium content of the protective oxide scale and decreases the oxide thickness. Applied stress, however acts to increase oxide thickness and decrease the chromium content of the oxide scale.

Introduction

The nickel-based alloy 600 (Ni-16Cr-9Fe) has been used for steam generator (SG) tubing in pressurized water reactors (PWR). This alloy is susceptible to intergranular stress corrosion cracking (IGSCC) in primary water. The higher chromium alloy 690 (Ni-30Cr-9Fe), shows better resistance to IGSCC[1] and is currently being used in replacement steam generators and in the manufacture of new SG's. To date, the improved resistance of alloy 690 has not yet been clearly explained.

Coriou *et al.* are the first to examine the effects of chemical composition on stress corrosion cracking in high temperature water [2]. Recent studies have shown that chromium has a beneficial effect on the resistance to IGSCC [3,4]. Determining the specific cause behind the beneficial role of chromium is difficult because of the large number of factors influencing IGSCC behaviour. Chromium influences the formation of a surface film. The oxide film is more protective and has a better mechanical resistance for chromium contents higher than 17% [5]. It has also been shown that the passivity and the repassivation rates in environments increase with Cr content [5,6]. For chromium contents above 12% the alloy is given the designation "stainless" For equivalent corrosion times, the oxide layer that develops in alloy 600 is thicker than that developed in the 690 alloy [7,8]. The creep and deformation rates are decreased by the hardening effect of chromium [4,9,10], for example, Vaillant *et al.* observed a decrease in creep rate by a factor of 2 for an increase in chromium content from 15% to 30% for similar grain boundary precipitation and thermal treatment conditions. The effect of Cr on IGSCC has been also attributed to the grain boundary chromium level [11]. This study is undertaken in order to determine the effect of chromium and plastic deformation on the oxide films formed on Ni-xCr-9Fe ($5 < x < 30$ wt%) alloys corroded in primary water.

Alloys and experimental procedures

Seven different alloys are prepared by the steel maker TECPHY with compositions ranging from low (5 wt%) to high (30 wt%) chromium contents (**Table 1**). This range spans the composition of the industrial alloys (alloy 600 (15%) and alloy 690 (30%). The content of alloying elements such as Fe, Ti, Al are maintained within the specification of alloys 600 and 690 in order to be comparable with the industrial products. The composition balance is done on nickel.

Reference	C	Ni	Cr	Fe	Ti	Al	Si	S
B283	0.021	Bal.	5.11	8.25	<0.005	0.015	0.126	0.006
B216	0.027	Bal.	10.02	10.55	<0.005	0.012	0.107	<0.001
B379	0.019	Bal.	14.96	10.07	0.24	0.07	<0.01	<0.001
B381	0.02	Bal.	19.98	10.11	0.24	0.07	<0.01	<0.001
B384	0.017	Bal.	24.99	10.12	0.24	0.09	<0.01	<0.001
B385	0.017	Bal.	27.13	10.19	0.24	0.08	<0.01	<0.001
B388	0.019	Bal.	30.01	10.13	0.24	0.08	<0.01	<0.001

Table 1. Chemical composition of the alloys studied (weight %).

For general corrosion tests, coupons are machined from the alloys in the form of rectangular bars 50mm long, 10mm width and 1mm thick. Slow strain rate tensile tests (SSRT) in pressurized water are realized on both cylindrical (diameter 4mm, gage length 80mm) and plate specimens (3mm width, 1mm thick and 20mm of gage length).

General corrosion tests are run for 1000 hours. Corrosion tests are performed in an isothermal loop. The primary PWR water is simulated by a solution of 1000 ppm boric acid and 2 ppm LiOH in demineralised water. The partial pressure of hydrogen is set to 0.17 bars. Pressure and temperature are fixed respectively at 18.5 MPa and 360°C, which represents an accelerated test compared to the conditions experienced in service. SSRT tests are performed in a static autoclave at 360°C and 15.0 Mpa in a solution representative of PWR primary water. The specimens are deformed to rupture under an imposed strain rate of $5\ 10^{-8}\ s^{-1}$, leading to test durations ranging from 350 to 3000 hours. The

surfaces of all specimens are polished down to grade 1200 grade SiC paper.
The oxide films are analyzed using scanning electron microscopy (SEM), analytical transmission electron microscopy (ATEM) and secondary ion mass spectrometry (SIMS). The corrosion products are characterized using a LEO SUPRA 35 SEM equipped with a Field Emission Gun (FEG) and In-Lens detector operated at 5 kV.

A TECNAI F20 FEG/TEM operating at 200 kV is used for all TEM imaging. Energy filtered electron transmission microscopy (EFTEM) images are acquired at 198 kV using a GATAN Image Filter (GIF), K ratio images are shown obtained with the two windows techniques. Energy dispersive X ray (EDX) analyses are performed in the scanning transmission mode, with a spot size random from 1 to 1.5 nm, and the specimen tilted to 20° towards the detector using automatic line scanning analysis. There are difficulties in quantifying oxygen concentrations using EDF methods as the pairs of Cr L lines (0.45-0.57keV) and O K lines (0.52 keV) can't be resolved due to the relatively poor energy resolution of the EDX detectors. As such the oxygen signal is not shown and is not used for determining the oxide composition, instead the percentage of the different oxides corresponds to the ratio of metallic compounds. The oxygen repartition is studied using energy loss filtered imaging. No surface preparation is used for SEM observations, TEM cross sections are prepared using conventional techniques. The first step is to cut a section of the surface and to embedded in a brass insert. Then the insert is sliced to obtain thin discs, these discs are polished mechanically to a final thickness of 80µm. A bowl-shaped depression is created with dimple grinding. The final ion-milling with GATAN Precise Ion Polishing System (PIPS) is used to produce electron transparent regions for TEM characterization. SIMS analyses are performed using a CAMECA IMS 4F, the abraded rate in the alloy is calibrated in order to set the depth under the metal-oxide interface at which the elemental images are taken .

Results and discussion

- Oxides on undeformed specimens

The microstructures of the external corrosion layer produced on coupons are first examined by SEM for the different alloys. The alloys presenting the lowest chromium contents (5 and 10%) exhibit oxides in filaments shaped on their surface. The filament density increases with decreasing chromium content until the surface is completely covered for the 5 wt% Cr alloy (Figure 1a).

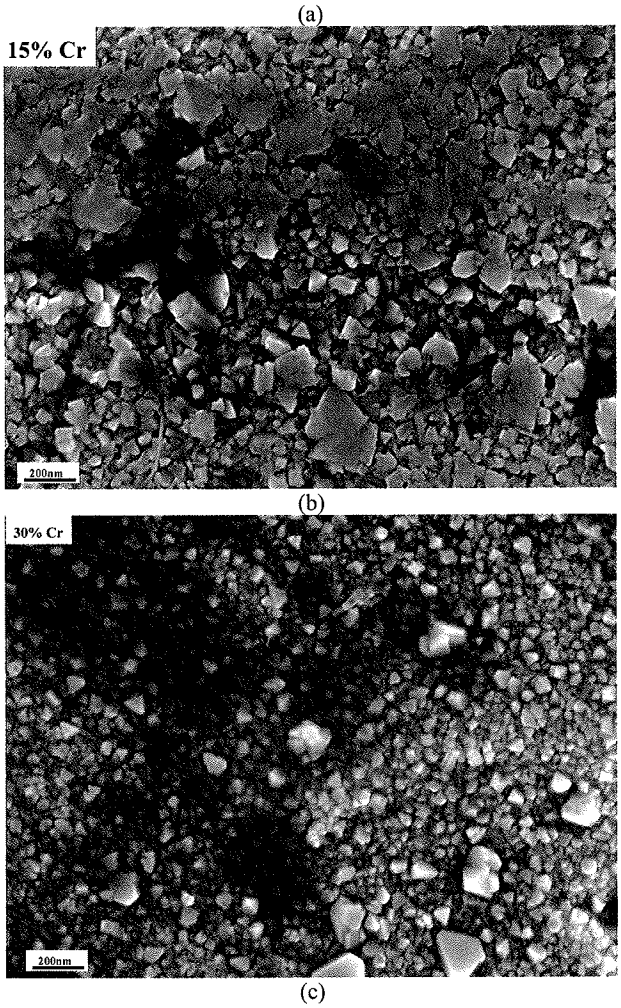

Figure 1. SEM images of the oxide scale developed in simulated primary water on alloys with various Cr contents (a) 5% Cr, (b) 15% Cr and (c) 30% Cr.

Two categories of filaments are detected; nickel-rich filaments, and filaments containing both iron and nickel (probably $NiFe_2O_4$ spinels). Beneath the filament layer small discrete crystallites are observed, as indicated by the white arrows in Figure 1a. The filaments disappear with increasing chromium content and are replaced by a distribution of crystallites as illustrated in Figures 1b (15% Cr) and 1c (30% Cr). The crystallites present a bimodal size distribution of small crystallites in the order of 10nm, and large ones ranging from 100 nm to few microns (randomly distributed) (Figure 1c). The average size of the small crystallites decreases with chromium content

The oxide scales are also observed in the cross-section using TEM in order to examine in more detail the different layers of the scale, both in structure and composition.

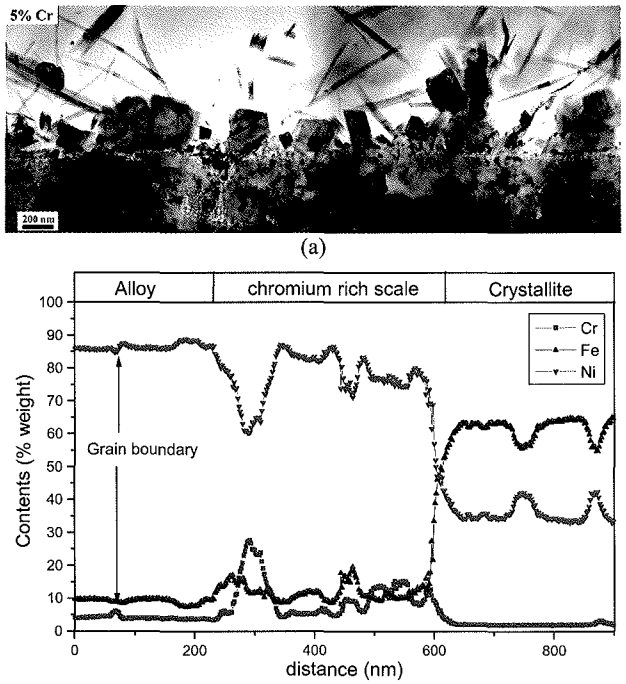

Figure 2. TEM cross-section of the oxide scale developed in simulated primary water in the 5% chromium alloy.

Figure 2 illustrates the entire thickness of the oxide formed on the 5% Cr alloy. The filaments observed in Figure 1a, can be seen on the coupon surface although they are somewhat damaged due to the TEM sample preparation. The crystallites seen in SEM are also visible beneath the filaments and do not form a continuous layer. An inner oxide layer can be seen below the crystallites. This consists of chromium rich oxide grains that have penetrated into the metal as opposed to oxide grains that have grown outwards from the metal surface.

The outer oxide layer formed on the 15% Cr alloy, is composed of the crystallites observed previously in SEM (Figure 3). This layer is not compact and an EDX scan indicates enrichment of the crystallites by Ni and Fe (see the EDX line scan in Figure 3). A 10nm thick inner oxide layer is observed enriched with chromium up to 50%. In this layer the impurities like titanium could segregate (see Figure 3). Chromium is depleted over a distance of approximately one hundred nanometres beneath the metal-oxide interface.

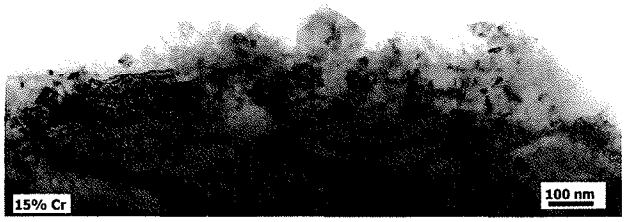

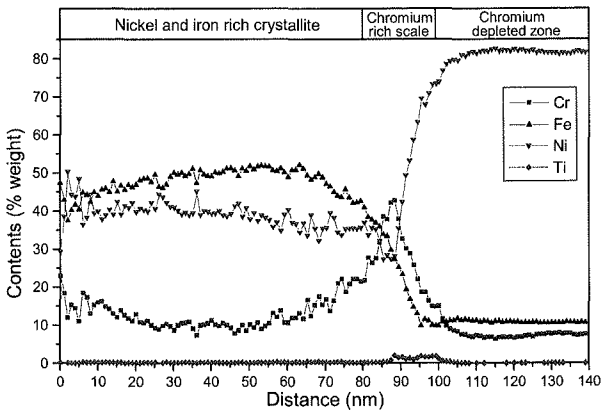

Figure 3. TEM cross-section of the oxide scale formed on the 15% Cr alloy in simulated primary water.

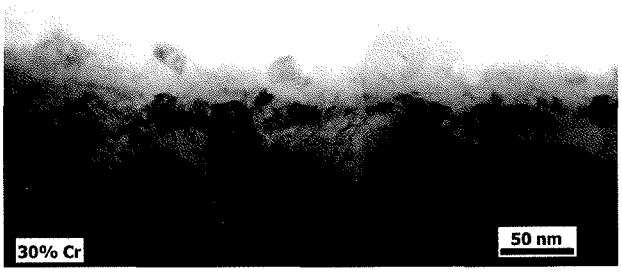

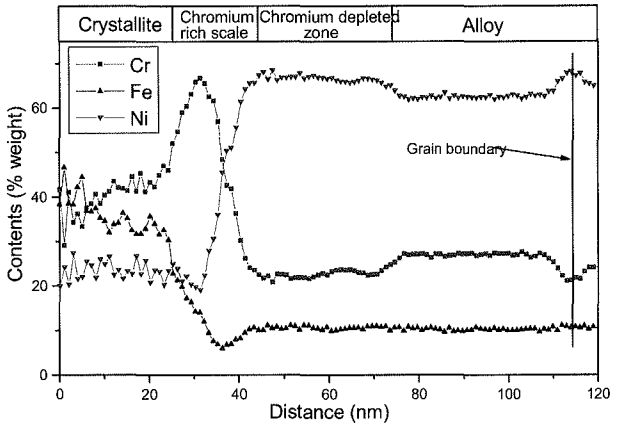

Figure 4. TEM cross-section of the oxide scale formed on the 30% Cr alloy in simulated primary water.

The layered structure of the oxide scale developed on the 30 % alloy is shown in Figure 4. The outer surface displays crystallites as observed by SEM (Figure 1.a). This layer is not continuous, consisting of discrete separated grains, meaning it is unlikely that this layer acts as a protective layer. A second layer, 10nm thick, consisting of very small oxide grains is observed below the outer surface. The structure of the oxide layers is more clearly defined in the X ray profile analysis (Figure 5). The outer crystallites are enriched in chromium and iron (40% of Cr and 40% of Fe). The second oxide layer is highly enriched in chromium, reaching levels of up to 70%. The parent metal is impoverished of chromium over a thickness of 30nm below the second oxide layer.

These features are observed on all alloys with chromium contents higher than 10 %. Table 2 summarises the characteristics (composition and dimensions) of the zone depleted of chromium as a function of chromium content. The EDX analysis shows that the external crystallites are progressively enriched in chromium at the expense of iron and nickel for alloys with increasing nominal chromium content. By contrast, the inner Cr rich layer behaved differently: a minimum chromium content is required to form this layer (~ 10 %), this layer being unchanged in thickness and composition for higher nominal chromium contents. These features are summarized in Table 2.

Chromium content	**5 %**	**10%**	**15%**	**20%**	**25%**	**30%**
Max. size of big crystallites	few µm	few µm	140 nm	90 nm	50 nm	50 nm
Composition of big crystallites	$NiFe_2O_4$ and Ni rich	$NiFe_2O_4$ and Ni rich	10% Cr 50% Fe 40% Ni	25% Cr 50% Fe 25% Ni	45% Cr 25% Fe 20% Ni	50% Cr 40% Fe 10% Ni
Thickness of Cr in the inner layer	100 to 200 nm	100 nm	5-10 nm	5-10 nm	5-10 nm	5-10 nm
Max. % of chromium in the inner layer[1]	25[2]	80	80	75	80	90
Max. depth of Cr in the depleted zone	-	500 nm	100 nm	~100 nm	~100 nm	60 nm

Table 2. Characteristics of the oxide layers appearing on coupons as a function of the chromium content of the alloy.

[1]This percentage corresponds the percentage chromium is given by the ratio of chromium to other alloying elements, it's not the real composition of the oxide, because the oxygen is not quantified.

[2] For the 5 % Cr alloy the inner oxide does not form a layer but instead is constituted by the penetration of large particles from place to place.

In order to identify the consequences of the corrosion process inside the alloys, chemical analysis of the coupons have been performed by SIMS in the "reversed mode". That is, the analysis is performed in image mode from the metal side of the oxide layer, and successive removals of the metal enabled a through thickness investigation of the distribution up to the oxide [12]. This procedure presents two main advantages as compared to classical SIMS analysis where the abrasion starts from the oxide to the metal: i) A flat clean surface can be obtained from the metal side in contrast with the rough outer oxide layer and ii) the sensitivity to oxygen can be adjusted to detect very small amounts of O atoms (The detector rapidly saturates in its detection of oxygen when starting from the outer oxide surface. Contamination of the metal by oxides is also avoided). The three images of Figure 5 are taken chronologically during such a "reversed" abrasion sequence, Figure 5a is 4.5µm under the metal oxide interface, to Figure 5c which is taken on the oxide scale itself. This analysis demonstrates that oxygen penetrates over large distances into the metal. It must be noted that the oxygen penetration is not uniform but it's localized at certain points in the microstructure. Further abrasion shows the correspondence of these points with the triple lines in the grain structure. These results complement the observations by SIMS performed by Newman et al [13], who detected chromium oxide at the grain boundary under the surface of alloy 600. The present results indicate the role of triple lines and the large penetrations of oxygen that can be observed (penetrations up to 9 µm are seen).

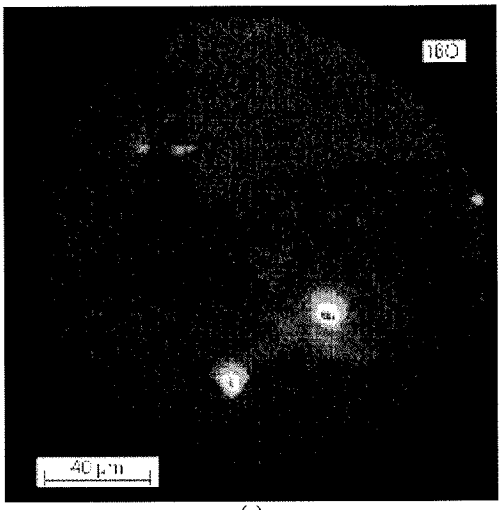

(a)

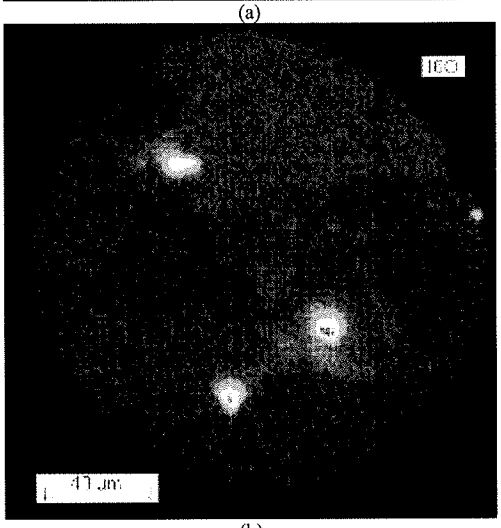

(b)

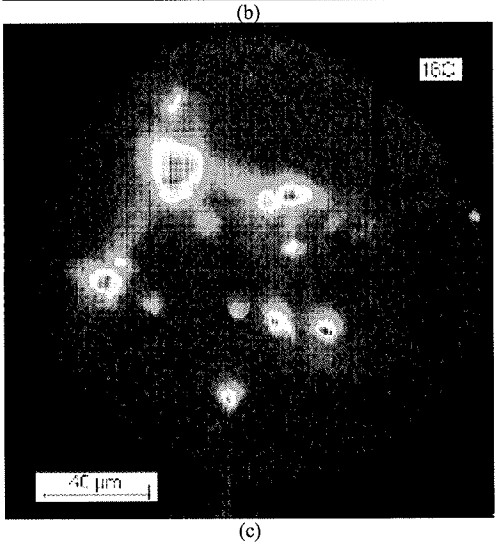

(c)

Figure 5. SIMS images of the oxygen signal during "reversed abrasion" showing the deep penetration of oxygen at the triple lines and grain boundaries of the 20% Cr alloy. The images correspond respectively to the depth under the metal surface: (a) 4.5 µm, (b) 1.9 µm, (c) 0.3 µm.

The overall consequences of corrosion on nickel-based alloys is schematized in Figure 6. An outer oxide layer consisting of large sparse crystallites and a more uniform distribution of small crystallites is seen. Below the outer layer is a thin compact layer of chromium rich oxide (chromium can be enriched up to 90 %). Beneath this layer, the alloy is depleted in chromium over a distance of a few tens of nanometres. An "affected zone" is observed in the metal, which takes on the appearance of a heavily deformed and fine grained microstructure as reported in the literature [14]. The deep penetration of oxygen at the triple junctions of grain boundaries is also indicated. This schema is only valid for alloys with a chromium content higher than 10 %. Below this composition numerous filaments are present on top of the oxide scale and the chromium rich oxide layer is not continuous.

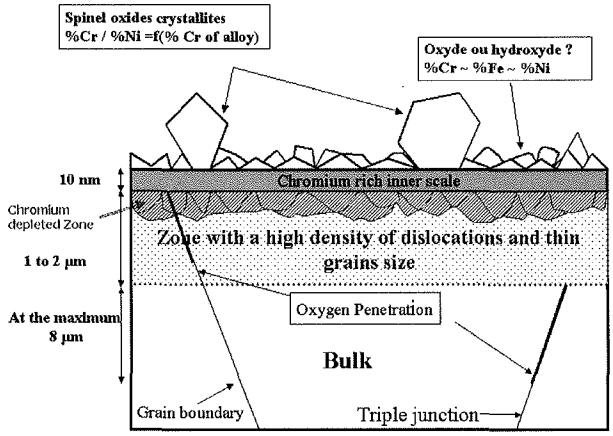

Figure 6. Schematic of the oxide structure observed for nickel based alloys with chromium contents above 10% oxidized in simulated primary water

- Oxides on deformed specimens

Complete characterization of the corrosion products on the SSRT specimens has also been performed. Figure 9 show the cross section of the 5% Cr alloy. The corrosion layers are strongly modified in comparison with the layers formed on coupon. The outer scale consists of oxide filaments, however the inner oxide is slightly enriched by Cr and Fe (up to 10% Cr and up to10% Fe).

Figure 8 shows the cross section of the 15 % Cr alloy as imaged using the jump ratio technique in GIF. The structure of the oxide scale on deformed material is strongly modified with respect to the unstressed sample. The oxide-metal interface, indicated by the dashed white line in the Fe ratio image, does not present a thin layer of Cr rich oxide (Figure 9). Instead oxygen penetrates more deeply into the metal to form Cr enriched oxide inside the parent metal. The structure of the oxide scale is similar to that developed in unstressed samples of lower Cr contents.

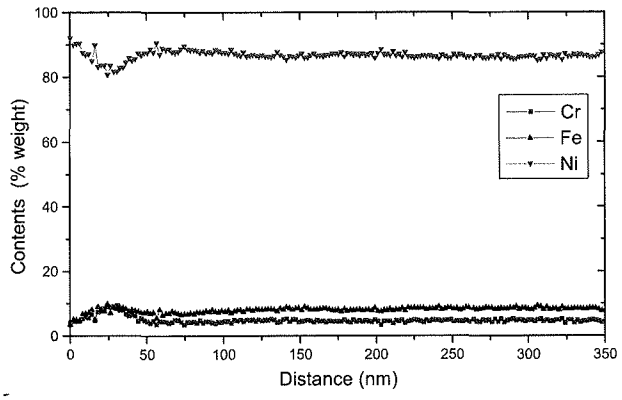

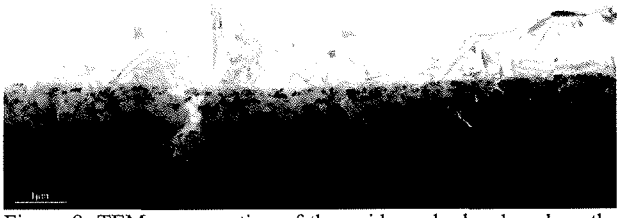

Figure 8. TEM cross-section of the oxide scale developed on the 5% Cr tensile specimen tested in simulated primary water.

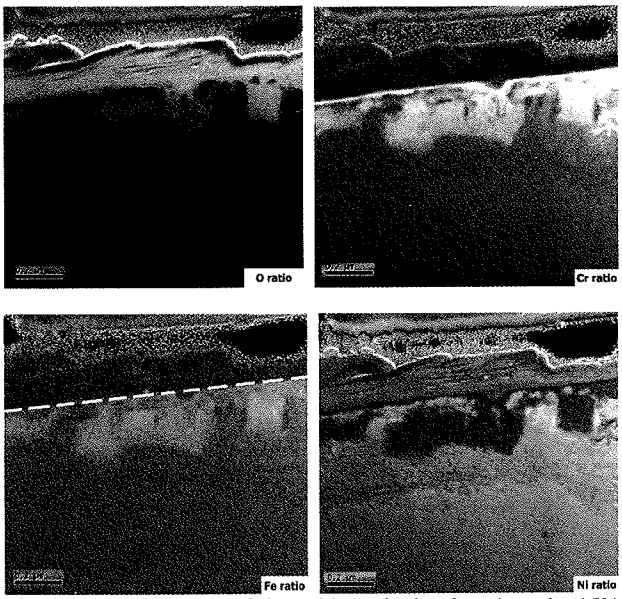

Figure 9. Cross section of the oxide scale developed on the 15% Cr alloys during SSRT testing to rupture (exposure time: 2500 hours) as observed in EFTEM.

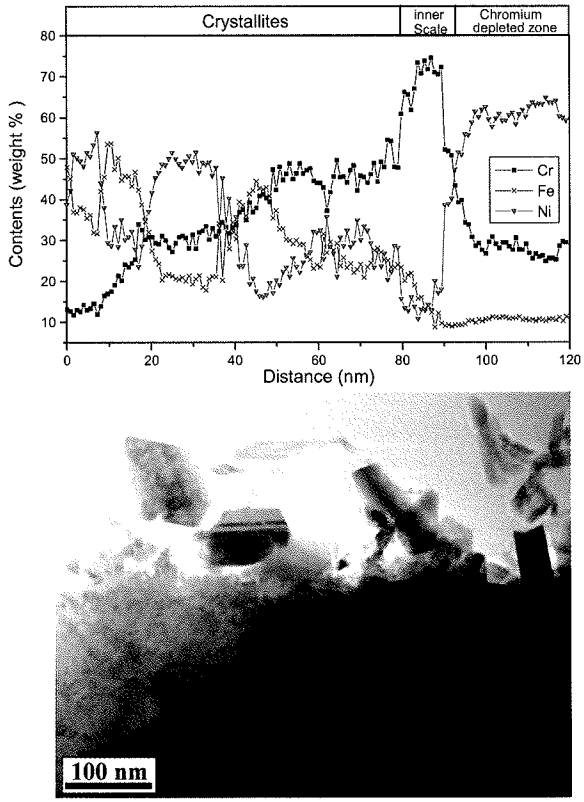

Figure 10. Cross section of the oxide scale developed on 30% Cr alloys during SSRT (exposure time: 2500 hours).

The layered structure of the oxide scale developed on the SSRT specimen of the 30 % alloys is shown in Figure 10. At the outer surface, crystallites of about a hundred nanometers size are seen. The inner oxide layer consists of a layer enriched in chromium (up to 70%), as illustrated by the line scan crosses on Figure 10. This layer is about 10 nm thick. A 20nm layer impoverished of chromium is observed in the parent metal below the metal oxide interface.

These results confirm the general tendency of plastic deformation to weaken the role of Cr in the development of the Cr oxide protective layer. A few observations have been also undertaken to characterize the structure of oxide within cracks developed during tensile tests. Such observations indicate that the structure of oxides and alloy modifications within cracks are very different from what happens at the free surface. Two explanations for this difference can be given : i) the confinement of the corroding medium in the crack alters the electro-chemical conditions with respect to the surface and ii) mechanical stresses are strongly concentrated at the crack tip resulting in modifications of the corrosion rate. These finding highlight the essential importance of characterizing the SCC directly in the crack, in agreement with the observations by Thomas et al. [15]. Recent work in this view showed that such observation may be very useful for discriminating between the different mechanisms that may operate during laboratory or in service stress corrosion cracking of nickel based alloys [16].

CONCLUSION

The consequence of corrosion in high temperature water on nickel based alloys as a function of chromium content has been characterized using SEM, TEM and SIMS. All alloys formed a non-continuous external layer of crystallites (non protective). For alloys above 10% chromium a continuous and compact layer of chromium oxide develops that covers the metal surface. The penetration of oxygen under the oxide scale along triple junctions is evidenced by SIMS imaging, this penetration may reach several micrometers. The SSRT tests showed that chromium content has a strong influence on the rate of oxide growth. Plastic deformation is shown to have a significant influence on the structure of the corrosion film. In particular the detrimental influence of strain on the protective chromium oxide layer has been demonstrated. The designation "stainless" can be linked up to the existence of oxide rich inner layer. Further paper will deal with the effect of chromium on IGSCC behaviour and oxide growth within cracks.

References

[1] K. SMITH, A. KLEIN, P. SAINT-PAUL and J. BLANCHET, proceedings of second international Symposium In Environmental Degradation of Materials In Nuclear Power Systems-Water reactors, pp12-1 to 10, NACE, 1989.

[2] H. CORIOU, L. GRALL, Y. LEGALL, S. VETTIER, "SCC of Inconel in high temperature water", 3rd metallurgy symposium, Saclay, France, p.161, 1960.

[3] T. YONEZAWA, N. SASAGURI, K. ONIMURA, "Effects of metallurgical factors on stress corrosion cracking of Ni-base alloys", Japan Atomic Industrial Forum, vol. 2, p.490, 1988.

[4] G.S. WAS, "Micromechanical and microstructural effects on SCC of nickel base alloys", PARKINS symposium on fundamental aspects of stress corrosion cracking, 1991.

[5] T.M. ANGELIU, G.S. WAS, "The effect of chromium, carbon and yttrium on the oxidation of nickel-base alloys in high temperature water", Journal of Electrochemical. Society, vol.140, p.1877, 1993.

[6] K. YAMANAKA, J. MURAYAMA, proceedings of fourth international symposium on environmental degradation of materials in nuclear power systems-water reactors, Houston, p.96 1989.

[7] L. GUINARD, O. KERREC, D. NOEL, S. GARDEY and F. COULET, Water Chemistry of Nuclear Reactor Systems 7, BNES, Bournemouth, 62, 1996.

[8] F. CARRETTE, « Relâchement des produits de corrosion des tubes en alliage 690 de générateur de vapeur du circuit primaire des réacteurs à eau pressurisée », Ph-D Thesis (in French), *INP Toulouse,* 2002.

[9] G.S. WAS, "Deformation and intergranular cracking behaviour of Ni-Cr-Fe alloys at high temperature", EPRI Airlie Workshop, *Warrenton*, 1993.

[10] F. VAILLANT, J.D. MITHIEUX, O. DE BOUVIER, D. VANCON, G. ZACHARIE, "Influence of chromium content and microstructure on creep and PWSCC resistance of nickel base alloys", Proceedings 9th Symposium on environmental degradation of materials in nuclear power system, 1999.

[11]. J.J. KAI, G.P. YU, C.H. TSAI, M.N. LIA, and S.C. YAO, "The Effects of Heat Treatment on the Chromium Depletion, Precipitate Evolution, and Corrosion Resistance of Inconel Alloy 690" Metallurgical Transactions A., Vol.20A, p.2057, 1989.

[12] J. PANTER; B. VIGUIER; J.M. CLOUÉ, J.; M. FOUCAULT, P. COMBRADE, and E. ANDRIEU; « Influence of

oxide films on primary water stress corrosion cracking initiation of alloy 600 », *Journal of Nuclear Materials*, submitted 2005.
[13] R.C. NEWMAN; T.S. GENDRON and P.M. SCOTT; "Internal oxidation and embritlement of Alloy 600", *Ninth International Symposium on Environment Degradation of Materials in NPS-WR, Newport Beach, CA, USA 1-5 Aug 1999, The TMS* pp 79 – 93, 2000.
[14] F. CARRETTE, M.C. LAFONT, G. CHATAINIER, L. GUINARD and B. PIERAGGI, « Analysis and TEM examination of corrosion scales grown on Alloy 690 exposed to pressurized water at 325 C » *Surface and Interfaces analysis.*, 34:, pp. 135–138, 2002.
[15] L. THOMAS and S. BRUEMMER, "High resolution analytical electron microscopy characterization of corrosion and cracking at buried interfaces", *Surface and Interfaces analysis*, **31**, p.571-581, 2001.
[16] F. DELABROUILLE, "Caractérisation par MET de fissures de corrosion sous contrainte d'alliages à base de nickel : influence de la teneur en chrome et de la chimie du milieu" *Ph –D Thesis (in French), INP Toulouse*, 2004.